Electrochemistry Communications 180 (2025) 108056

Contents lists available at ScienceDirect

Electrochemistry Communications

journal homepage: www.elsevier.com/locate/elecom

# Modeling current density and SoC distribution of all-solid-state lithium-ion batteries

Zhenya Wang [a,b,c], Dmitri L. Danilov [b,d,*], Jingjing Zhou [a], Meng Zheng [a], Yi Huang [a], Tao Chen [a], Rüdiger-A. Eichel [b,c], Peter H.L. Notten [b,d,e,*]

[a] China Automotive Engineering Research Institute Co., Ltd, Chongqing, 401122, China
[b] Forschungszentrum Jülich (IET-1), D-52425 Jülich, Germany
[c] Institute of Physical Chemistry, RWTH Aachen University, D-52074 Aachen, Germany
[d] Eindhoven University of Technology, P.O. Box 513, Eindhoven 5600 MB, the Netherlands
[e] Centre for Clean Energy Technology, University of Technology Sydney, Broadway, Sydney, NSW 2007, Australia

ARTICLE INFO

*Keywords:*
All-solid-state batteries
Current collectors
Discretization
Current density distribution

ABSTRACT

Researchers have conducted in-depth investigations into lithium-ion battery models. However, a notable limitation of existing models lies in the assumption of infinitely conductive current collectors, which compromises simulation accuracy. Herein, we present a model that explicitly accounts for current collector resistance, employing Kirchhoff's circuit laws and a suitable discretization method to characterize the associated current density and SoC distribution in all-solid-state thin-film batteries. Simulation results demonstrate that the highest SoC occurs near the charging tab, leading to preferential full-charge in this region. Intriguingly, when charging is interrupted at this stage, the battery enters a self-balancing state: the state of charge SoC near the tab gradually decreases. At the same time, SoC in other regions increases, culminating in a homogeneous SoC across the entire battery. This phenomenon reflects the underlying process of lithium-ion redistribution. Additionally, a larger resistance disparity between cathodic and anodic current collectors creates an inhomogeneous current density distribution, thereby accelerating localized battery aging. The approach adopted by our model exhibits broad generality and can be readily adapted to other battery types.

## 1. Introduction

With the extensive use of fossil fuels such as coal, oil, natural gas, and nuclear fission, the degree of modernization in human society and the level of the global economy have been remarkably enhanced. However, environmental degradation induced by excessive energy exploitation has become increasingly severe [1,2]. Lithium-ion batteries are increasingly favored as promising electrochemical energy storage systems due to their high energy density and environmental friendliness. Nevertheless, the stable temperature range of organic electrolytes used in conventional lithium-ion batteries is relatively narrow and thus prone to safety accidents [3,4]. A promising approach is the production of all-solid-state batteries (ASSBs), where flammable liquid electrolytes are replaced by a solid electrolyte, thereby eliminating such issues. That could potentially offer better electrochemical performance and avoid hazardous electrolyte leakage [5–8]. Therefore, ASSBs are appropriate for industry applications, such as electric vehicles and medical implants, which are generating increasing research interest in academia at the same time.

Modeling ASSBs is beneficial for further understanding and improving the performance of batteries, which has drawn considerable attention from researchers. Nevertheless, a critical limitation of prevailing models, such as Neumann-type or Nernst-Planck-type models [9–12], lies in the assumption of infinitely conductive current collectors. The electronic part in current collectors was not simulated explicitly [11,13–16]. In fact, the current collector's resistance leads to significant voltage drops in ASSBs [17–20]. Paradoxically, despite this known effect, the influence of current collector resistance on current density and state of charge (SoC) distribution in ASSBs remains underexplored. Existing studies have primarily focused on electrical constriction resistance in liquid-based batteries [21–24], with only sporadic investigations into ASSB systems. It is worth noting that the inhomogeneous current density and SoC distribution of ASSBs trigger partial overcharge or over-discharge, insufficient use of the electrodes,

* Corresponding authors at: Forschungszentrum Jülich (IET-1), D-52425 Jülich, Germany.
*E-mail addresses:* d.danilov@fz-juelich.de (D.L. Danilov), p.h.l.notten@tue.nl (P.H.L. Notten).

https://doi.org/10.1016/j.elecom.2025.108056
Received 11 August 2025; Received in revised form 19 September 2025; Accepted 22 September 2025
Available online 23 September 2025

and degradation of the electrodes, thus affecting the durability and safety of batteries [22,23,25]. Additionally, investigating them via experimental or conventional modeling is relatively cumbersome and complex, demanding substantial resources.

Herein, the resistance of current collectors was taken into account. The current density and SoC distribution of all-solid-state thin-film batteries have been modeled using Kirchhoff's circuit laws and a facile discretization method. The influence of varying current collector resistances on current density and SoC profiles is systematically investigated. The proposed modeling approach exhibits remarkable generality and computational efficiency, enabling its direct application to other battery types. More significantly, this framework serves as a critical enhancement for improving the predictive accuracy of existing lithium-ion battery models.

## 2. Model development

The spatial-temporal distributions of electronic currents, ionic currents, and battery SoC during the charging process are numerically simulated using a discretization method under the assumption of Kirchhoff's circuit law. The discretization approach involves partitioning the entire battery into a finite number of sub-cells, enabling detailed simulations of electrochemical behaviors within each sub-cell. Fig. 1 shows the schematic diagram of an all-solid-state thin-film battery. The tabs for charging and discharging are located at the lower left ($I_{in}$) and lower right ($I_{out}$) of the battery, respectively, on different layers. The red dashed lines indicate it is divided into four sub-cells, and each rectangle represents a sub-cell. In the first step, it is divided into $2 \times 2$ models, and the electrochemical state of all sub-cells determines the distribution of the whole battery. Eventually, the discretization process will become more refined, and the distribution should become more accurate, as illustrated in Fig. 1 (b).

The general approach to battery modeling encompasses both the thermodynamic and dynamic aspects. The thermodynamic part determined the electromotive force (EMF) or equilibrium voltage, while the dynamic part is related to the overpotential, shown as

$$\eta = E^{bat} - E^{EMF} \approx I \cdot R_{\text{int}}, \tag{1}$$

where $\eta$ represents the overpotential, $E^{bat}$is the battery voltage, $E^{EMF}$ is the equilibrium voltage, and $R_{\text{int}}$ denotes the internal resistance. This proposed model is simple and only contains EMF as well as internal resistance, which involves the electronic part of the battery. Commercial all-solid-state thin-film batteries with a capacity of 0.7 mAh were used for this model. The EMF data and the internal resistance of the battery can be obtained and calculated from reference [13].

Firstly, the lithium-ion battery was divided into four sub-cells using the discretization method. Fig. 2 illustrates the equivalent circuit diagram of the $2 \times 2$ model. Four sub-cells were marked as (1), (1, 2), (1, 2), and (2). Corresponding to the actual situation in the all-solid-state thin-film battery of Fig. 1, there is an input current at the sub-cell (1) in the lower left corner. All currents supplied to the cells via wires were utilized in the main storage reactions of four-component sub-cells. The output current is located at the sub-cell (1, 2) in the lower right corner of the other layer. It can be observed that this equivalent circuit diagram includes the equilibrium voltages of the sub-cell, the internal resistance, electronic currents, and ionic currents. The arrows represent the assumed direction of currents. All nomenclatures are explained in Fig. 2. Unlike most existing models, the resistance of the current collector is not ignored in this model. Specifically, the blue rectangles in the diagram represent the resistance of the platinum current collector for the cathodic part, and the red rectangles represent the resistance of the copper current collector for the anodic part. The primary objective is to obtain the distribution of electronic currents, ionic currents, and battery SoC during the charging process.

Kirchhoff's current law and voltage law are applied to each node and loop of the circuit:

$$\begin{aligned}
-i_{1112}R_{1112} - E_{12} - j_{12}R_{12} + i'_{1112}R'_{1112} + j_{11}R_{11} + E_{11} &= 0\\
-i_{1121}R_{1121} - E_{21} - j_{21}R_{21} + i'_{1121}R'_{1121} + j_{11}R_{11} + E_{11} &= 0\\
-i_{2122}R_{2122} - E_{22} - j_{22}R_{22} + i'_{2122}R'_{2122} + j_{21}R_{21} + E_{21} &= 0\\
-i_{1222}R_{1222} - E_{22} - j_{22}R_{22} + i'_{1222}R'_{1222} + j_{12}R_{12} + E_{12} &= 0\\
I_{in} - i_{1121} - i_{1112} - j_{11} &= 0\\
i_{1112} - j_{12} - i_{1222} &= 0\\
i_{1121} - j_{21} - i_{2122} &= 0\\
i_{2122} + i_{1222} - j_{22} &= 0\\
j_{11} - i'_{1121} - i'_{1112} &= 0\\
j_{21} + i'_{1121} - i'_{2122} &= 0\\
i'_{2122} + j_{22} + i'_{1222} &= 0\\
i'_{1112} + j_{12} - i'_{1222} &= I_{out}
\end{aligned} \tag{2}$$

Eq. (2) can be written in the matrix form $AX = B$, where

$$A = \begin{pmatrix}
R_{11} & -R_{12} & 0 & 0 & -R_{1112} & 0 & 0 & 0 & R'_{1112} & 0 & 0 & 0\\
0 & 0 & R_{21} & -R_{22} & 0 & -R_{2122} & 0 & 0 & 0 & R'_{2122} & 0 & 0\\
R_{11} & 0 & -R_{21} & 0 & 0 & 0 & -R_{1121} & 0 & 0 & 0 & R'_{1121} & 0\\
0 & R_{12} & 0 & -R_{22} & 0 & 0 & 0 & -R_{1222} & 0 & 0 & 0 & R'_{1222}\\
-1 & 0 & 0 & 0 & -1 & 0 & -1 & 0 & 0 & 0 & 0 & 0\\
0 & -1 & 0 & 0 & 1 & 0 & 0 & -1 & 0 & 0 & 0 & 0\\
0 & 0 & -1 & 0 & 0 & -1 & 1 & 0 & 0 & 0 & 0 & 0\\
0 & 0 & 0 & -1 & 0 & 1 & 0 & 1 & 0 & 0 & 0 & 0\\
1 & 0 & 0 & 0 & 0 & 0 & 0 & 0 & -1 & 0 & -1 & 0\\
0 & 1 & 0 & 0 & 0 & 0 & 0 & 0 & 1 & 0 & 0 & -1\\
0 & 0 & 1 & 0 & 0 & 0 & 0 & 0 & 0 & -1 & 1 & 0\\
0 & 0 & 0 & 1 & 0 & 0 & 0 & 0 & 0 & 1 & 0 & 1
\end{pmatrix}, \tag{3}$$

$$X = \begin{pmatrix} j_{11} \\ j_{12} \\ j_{21} \\ j_{22} \\ i_{1112} \\ i_{2122} \\ i_{1121} \\ i_{1222} \\ i'_{1112} \\ i'_{2122} \\ i'_{1121} \\ i'_{1222} \end{pmatrix} \tag{4}$$

$$B = \begin{pmatrix} E_{12} - E_{11} \\ E_{22} - E_{21} \\ E_{21} - E_{11} \\ E_{22} - E_{12} \\ -I_{in} \\ 0 \\ 0 \\ 0 \\ 0 \\ I_{out} \\ 0 \\ 0 \end{pmatrix}. \tag{5}$$

The input current is 1C and will be interrupted immediately when one of the sub-cells is fully charged, allowing for the observation of the SoC of all sub-cells and their evolution over time. The evolution of SoC is shown in Eq. (6)

$$SoC(t + \Delta t) = SoC(t) + \frac{j\Delta t}{(Q_{\max}/(NM))}, \tag{6}$$

where $Q_{max}$ indicates the maximum capacity of the battery and NM is the number of sub-cells. Therefore, the majority of parameters, such as EMF, electronic currents, ionic currents, and SoC, will become dependent on time. Assuming all sub-cells have the same initial process, the linear eqs. (2) could be solved.

Next, consider the continuity equation and normalization. Fig. 3 shows a diagram of the inflow and outflow currents. The coordinates of the battery are shown in the figure, along with the height $\Delta z$. The balance between fluxes should be written out. The electronic current is divided into two components, i.e., $i_x$ and $i_y$. Taking the midpoint as a base, the incoming flux is subtracted from the outgoing flux and multiplied by the surface area. The surface area on the x component is $\Delta z\Delta y$, while on the y component is $\Delta z\Delta x$. What comes out (in minus) should be equal to what had been generated inside, i.e., the ionic current

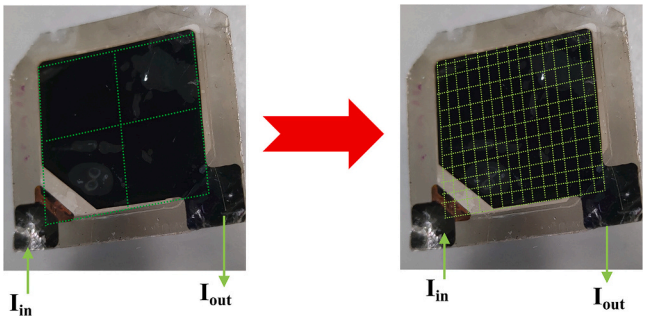


**Fig. 1.** Layout of discretization for an all-solid-state thin-film battery.

density times the volume of the battery, as written in Eq. (7).

$$\left[i_x\left(x + \Delta x, y + \frac{\Delta y}{2}\right) - i_x\left(x, y + \frac{\Delta y}{2}\right)\right]\cdot\Delta y\Delta z + \left[i_y\left(x + \frac{\Delta x}{2}, y + \Delta y\right) - i_y\left(x + \frac{\Delta x}{2}, y\right)\right]\cdot\Delta x\Delta z = j\left(x + \frac{\Delta x}{2}, y + \frac{\Delta y}{2}\right)\Delta x\Delta y\Delta z. \tag{7}$$

Then everything is divided by $\Delta x\Delta y\Delta z$, and the result is shown in Eq. (8).

$$\frac{\left[i_x\left(x+\Delta x, y+\frac{\Delta y}{2}\right) - i_x\left(x, y+\frac{\Delta y}{2}\right)\right]}{\Delta x} + \frac{\left[i_y\left(x+\frac{\Delta x}{2}, y+\Delta y\right) - i_y\left(x+\frac{\Delta x}{2}, y\right)\right]}{\Delta y} = j\left(x+\frac{\Delta x}{2}, y+\frac{\Delta y}{2}\right). \tag{8}$$

In the limit where $\Delta x$ and $\Delta y$ tend to 0 ($\Delta x \to 0$ and $\Delta y \to 0$), the equation can be simplified to Eq. (9) and Eq. (10). This equation can also be written in the form of the integral shown in Eq. (11). The currents in the horizontal direction should be divided by $\Delta x$. In contrast, the currents in the vertical direction should be divided by $\Delta y$ so that the normalization is completed.

$$\frac{\partial i_x}{\partial x} + \frac{\partial i_y}{\partial y} = \frac{j(x,y)}{\Delta z}, \tag{9}$$

$$div\left(\vec{i}\right) = \frac{j}{\Delta z}, \tag{10}$$

$$\oint\!\!\!\oint \vec{i}\, d\vec{s} = \iiint j dv. \tag{11}$$

According to Maxwell's equations, Kirchhoff's voltage law can be obtained from the equation

$$0 = \oint\!\!\!\oint (\nabla \times E)\cdot\hat{n} ds = \oint \vec{E}\, d\vec{r} = \sum_i \int E_i dr = \sum_i E_i \int dr = \sum_i E_i L_i = \sum_i V_i, \tag{12}$$

where $\hat{n}$ indicates the normal vector and $L$ represents a short piece along the path.

In addition, $\vec{i}$ is defined as the electronic current density in the bottom current collector and $\vec{i}'$ as the electronic current density in the upper current collector. Its components are shown in Eq. (13)

$$\begin{aligned} \vec{i} &= (i_x, i_y), \\ \vec{i}' &= (i_x', i_y'). \end{aligned} \tag{13}$$

$\vec{r}$ represents the position, and its components are shown in Eq. (14)

$$\vec{r} = (x, y). \tag{14}$$

Applying Kirchhoff's law to the model with current collectors, as described in Eq. (2), it can be concluded that the voltage drop across the two current collectors is related to the voltage of the sub-cell. The battery voltage here is the summation of the EMF and the overvoltage. It seems that we have a directional derivative. The total voltage across the battery is position-dependent. Thus, Eq. (15) could be obtained.

$$\begin{aligned} \frac{\partial E}{\partial x} &= \rho' i_x' - \rho i_x, \\ \frac{\partial E}{\partial y} &= \rho' i_y' - \rho i_y. \end{aligned} \tag{15}$$

where $\rho$ and $\rho'$ represent the specific resistance of the cathodic current collector and the anodic current collector, respectively. On the right side, the only possibility is specific resistance times current density, because when specific resistance is multiplied by current density, the

result is voltage per meter. This formula can also be written in the form of a limit, as indicated by Eq. (16).

$$\lim_{\Delta x\to 0}\frac{E(x+\Delta x)-E(x)}{\Delta x}=\rho^{'}(x)i_x^{'}(x)-\rho(x)i_x(x),$$
$$\lim_{\Delta y\to 0}\frac{E(y+\Delta y)-E(y)}{\Delta y}=\rho^{'}(y)i_y^{'}(y)-\rho(y)i_y(y). \tag{16}$$

The equation related to the voltage over the battery should be discretized according to

$$\begin{aligned}E(x,y)&=EMF(x,y)+\eta(x,y)\\&=EMF(x,y)+j_{ion}(x,y)R_{ion}(x,y)\\&=EMF(x,y)+\frac{j(x,y)}{\Delta x\Delta y}[R_{ion}(x,y)\Delta x\Delta y]\\&=EMF(x,y)+J_{ion}(x,y)\rho_{ion}(x,y),\end{aligned} \tag{17}$$

where $j_{ion}$ and$R_{ion}$ indicate the ionic current and internal resistance, respectively. $J_{ion}$ is the ionic current density. The previous equations, as well as the matrix, are to be normalized by $\Delta x$ and $\Delta y$. The difference in currents from Kirchhoff's current law depends on the direction (horizontal or vertical) in which the difference is made. Moreover, the input current $I_{in}$ should also be normalized by

$$I_{in}=\int jds. \tag{18}$$

Generalizing the descriptions above, the matrix equation of arbitrary dimension and corresponding SoC/current distribution of an arbitrary model can be derived. All derivations have been verified via MATLAB. The battery can be divided into finer dimensions to obtain a more accurate SoC/current density distribution.

## 3. Experimental

Thin-film current collectors with tailored thicknesses were fabricated via physical vapor deposition PVD machine (Kurt J. Lesker, UK) using silicon wafers as substrates. Platinum (Pt) current collectors were deposited onto Si substrates through direct-current (DC) magnetron sputtering of Pt targets. The distance between the substrate and the target material is fixed at 15 cm. The sputtering process is conducted in an Ar atmosphere at a chamber pressure of 5 mTorr, with a sputtering power of 70 W. In contrast, copper (Cu) current collectors were thermally evaporated at a deposition rate of 1 Å·s$^{-1}$. The substrates were maintained at a rotational speed of 20 rpm to ensure homogeneous film deposition. Following fabrication, current collectors with nominal thicknesses of 100 nm and 200 nm were obtained. The thickness of the samples was verified using a surface profilometer (Bruker, USA), and the resistance of the current collectors was characterized using a four-point probe device (Ossila, UK).

## 4. Results and discussion

The 2 × 2 model is initially simulated as the starting point. The SoCs of all sub-cells over time are shown in Fig. 4 (a). The battery will be fully charged after approximately 1 h, as the magnitude of the input current is 1C. At this time, the input current is interrupted. It can be concluded that the sub-cell (1) closest to the charging tab is the first to be fully charged. The sub-cell (2) located away from the charging tab is the slowest to charge due to the different path of the currents. Fig. 4 (b) illustrates the enlarged section showing the changes in SoC after the interruption. Interestingly, all sub-cells enter a self-balancing process. The SoC of sub-cell (1) is decreasing, while others are increasing, until the SoC of the entire battery becomes equal. That is essentially due to the redistribution of lithium ions. This process occurs because of the differences in the voltage among the discretized sub-cells, which correspond to their SoC levels. When charging stops, sub-cells with higher SoC (e.g., those near the tab) possess a higher voltage. This voltage potential difference drives

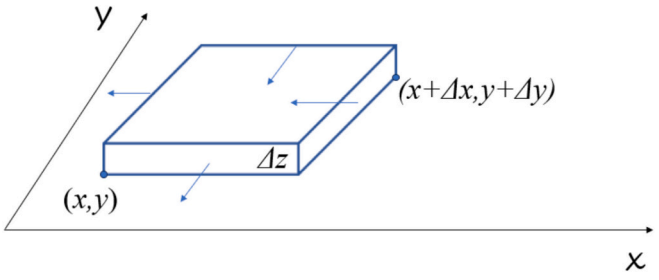


**Fig. 3.** Schematic diagram of incoming and outgoing currents for a sub-battery.

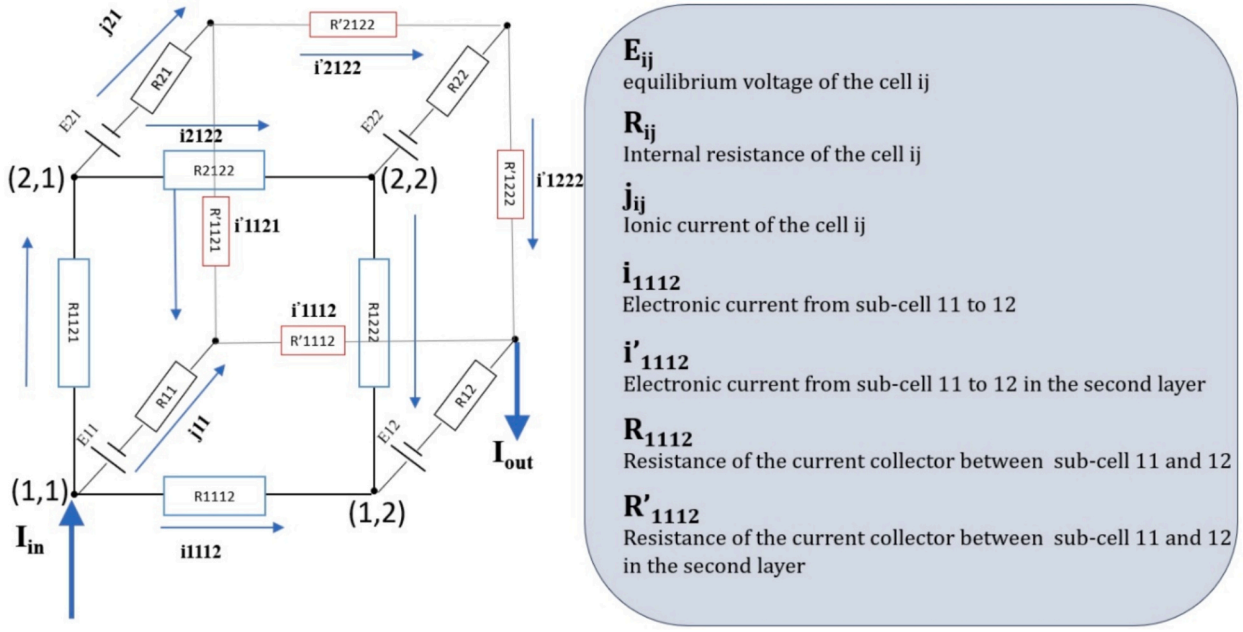


**Fig. 2.** Equivalent circuit diagram of the 2 × 2 model. The arrows represent the assumed direction of currents.

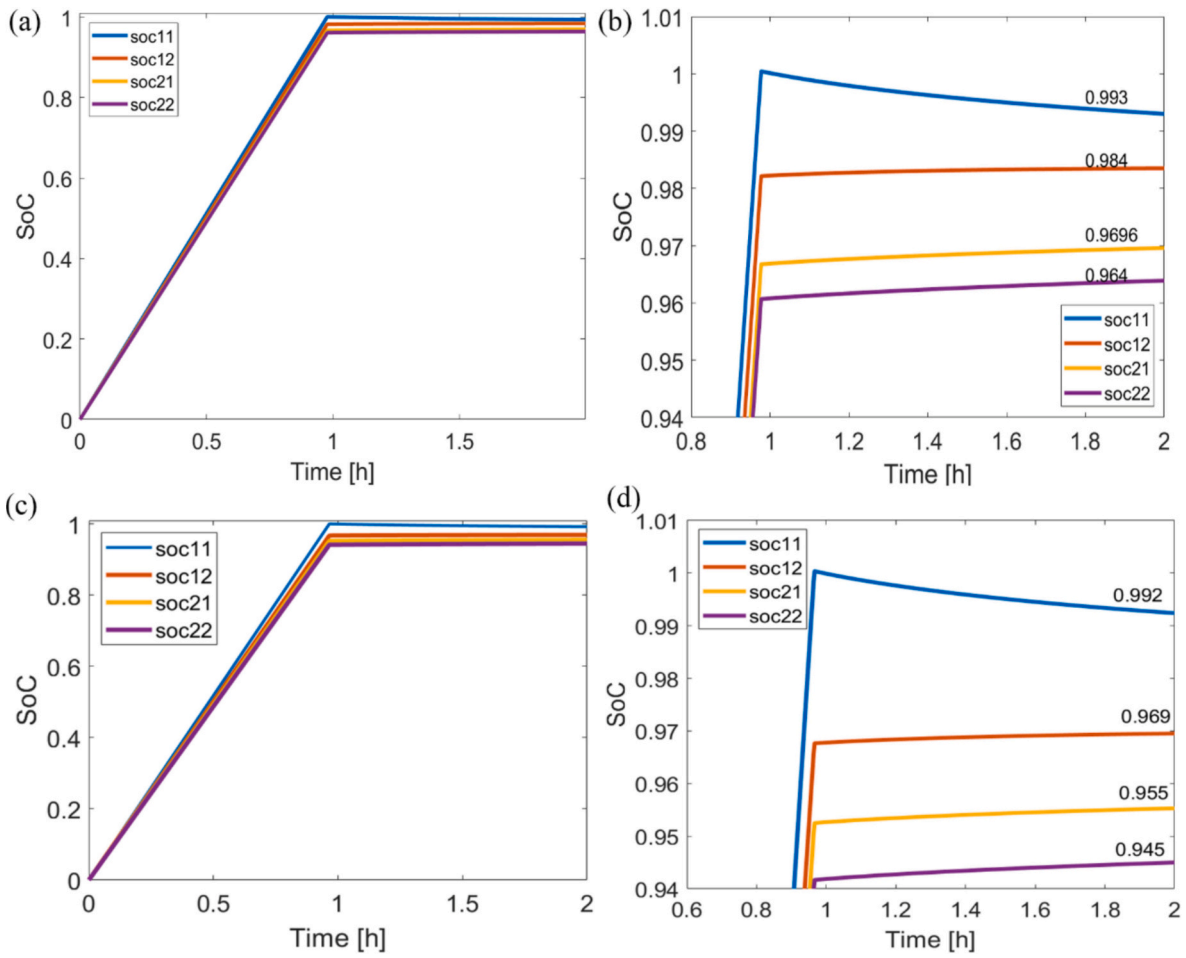


**Fig. 4.** (a) The change of SoC of all sub-cells over time, (b) the magnified part of SoC over time after the input current is interrupted, and (c) - (d) corresponding trend after increasing the resistance of the cathodic current collector.

an internal current flow from high-SoC regions to low-SoC regions through the network of electronic and ionic resistances that connect the sub-cells. This internal current flow continues until the voltage, and therefore the SoC, is equalized across all sub-cells, reaching an equilibrium state. This macroscopic current flow is the model's representation of the physical redistribution of lithium ions. It is worth noting that the resistance of cathodic and anodic current collectors should differ, as shown in Fig. 2, because platinum and copper have different resistivities. More importantly, their resistance affects the current density and SoC distribution.

Fig. 4 (c)-(d) demonstrate the spatiotemporal evolution of SoC for all sub-cells when the thickness of the Pt current collector is reduced from 200 nm to 100 nm. This observation correlates with the increased electrical resistance of the Pt current collector and the amplified resistance discrepancy between the Pt and Cu current collectors. Notably, the SoC discrepancies among sub-cells are significantly amplified, thereby reflecting the reduced homogeneity in current density and SoC distribution across the entire battery. As observed, sub-cell (1) exhibits a higher charge accumulation compared to all other sub-cells. That phenomenon can be attributed to the increased resistance encountered by electronic transport pathways, particularly the (1)→ (1, 2) and (1)→ (1, 2) transitions. The resulting impedance forces the system of governing equations to redistribute current flow preferentially through lower-resistance pathways. Specifically, current diverts from sub-cell (1) through ionic conduction channels, followed by diffusion from sub-cell (1′,1′) to the entire second layer, where resistive losses are minimized. That hypothesis is further validated by increasing the resistance even more, which accentuates the preferential current redistribution effect. In the asymptotic regime where the resistance of the bottom layer approaches infinity, the current distribution converges to a degenerate state wherein charge accumulation occurs exclusively within sub-cell (1).

Furthermore, the discretization becomes more refined to obtain an accurate SoC distribution of the entire battery. Fig. 5 illustrates the SoC distribution for the 15 × 15 model. As shown in Fig. 5 (a), an inhomogeneous distribution is observed. The area near the charging tab is fully charged first, while the SoC value is lower for the part away from the charging tab, owing to the different paths of the currents. After an hour of the self-balancing process, the SoC near the charging tab begins to decrease, while the rest of the area starts to increase, as illustrated in Fig. 5 (b). It can be inferred that after a period, the entire distribution map will become a horizontal plane, suggesting that the SoC value of the entire battery will be equal, and the current density distribution will become uniform. That is the redistribution process of lithium ions within the battery, unaffected by external factors. When the discretization reaches a satisfactory resolution, the SoC distribution across the entire battery becomes directly observable with intuitive clarity.

To further investigate the impact of current collector resistance on the SoC distribution, the resistance disparity between Pt and Cu current collectors is enlarged by reducing their thickness to 100 nm. As depicted in Fig. 5 (c), when a portion of the battery reaches full charge, the minimum SoC of the entire battery remains at approximately 0.93. This observation leads to a critical conclusion: a more pronounced resistance difference between cathodic and anodic current collectors exacerbates the inhomogeneity in SoC and current density distributions. Such inhomogeneity results in underutilization of electrode materials and

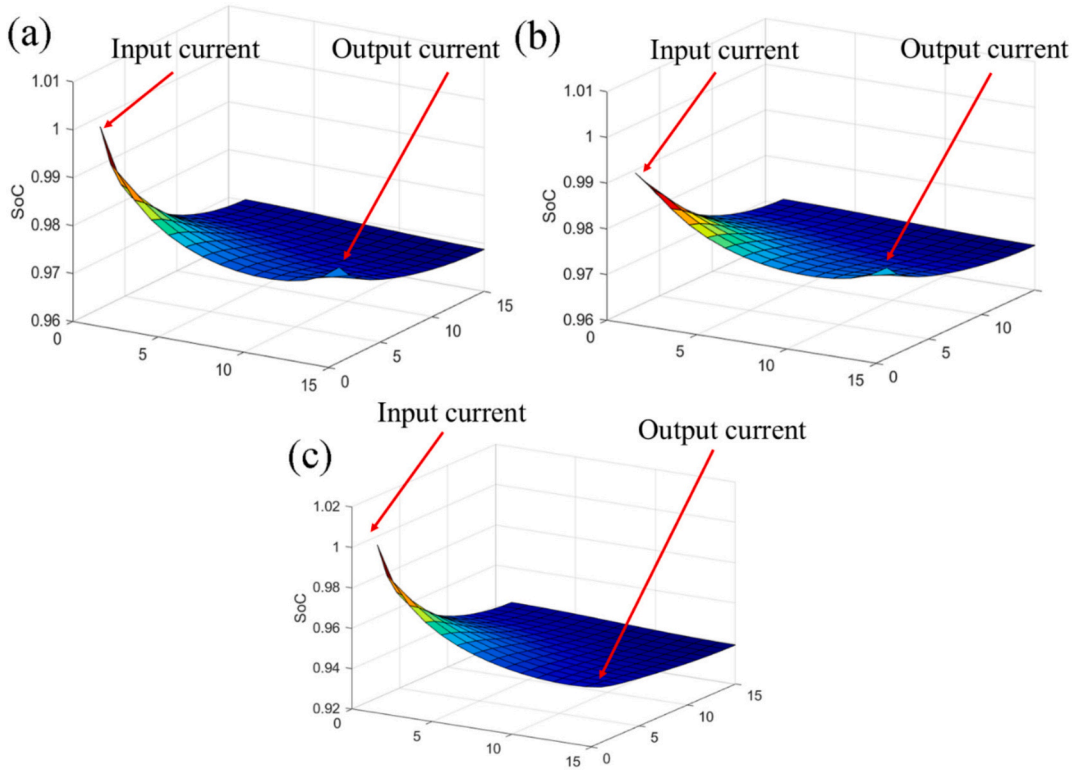


**Fig. 5.** (a) SoC distribution of a 15 × 15 model of the battery when one sub-cell is fully charged, and (b) after an hour of the self-balancing process. (c) SoC distribution after increasing the resistance difference between Pt and Cu current collectors.

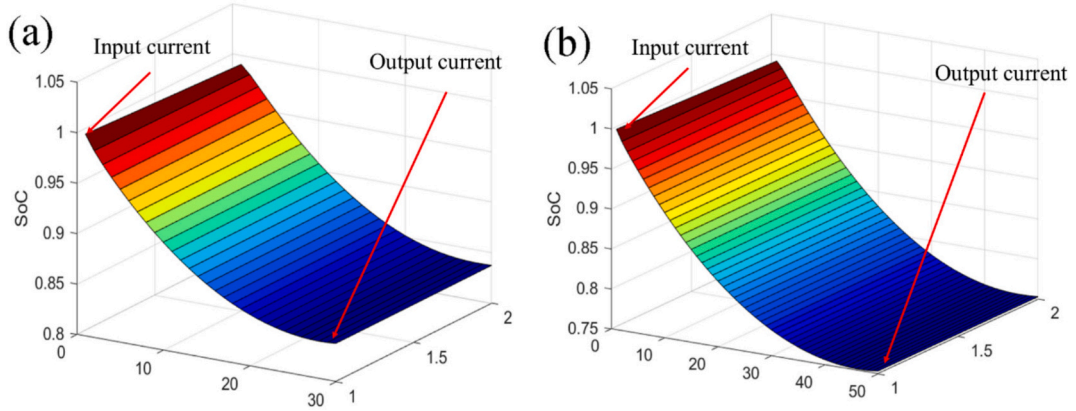


**Fig. 6.** SoC distribution at (a) 30:2 and (b) 50:2 aspect ratios of the battery.

localized over(*dis*)charge phenomena, thereby posing significant challenges to device durability and safety. Notably, the resistance variation is inherently linked to the geometric dimensions of the current collectors, offering valuable guidance for optimizing their structural design parameters.

In addition, the geometric proportions of current collectors of ASSBs are systematically varied to explore their influence on the current density distribution. As shown in Fig. 6, increasing the aspect ratio exacerbates the inhomogeneity of the SoC distribution. Specifically, the minimum SoC of the battery decreases from 0.83 to 0.75 after the aspect ratio changes from 30:2 to 50:2 when some areas have been fully charged. That indicates that current collectors with elongated strip geometries induce the most pronounced inhomogeneity of current density distribution, highlighting the critical role of aspect ratio in modulating charge distribution dynamics within ASSB architectures. Therefore, the battery manufacturers should pay attention to the aspect ratio or the tabbing design to optimize this issue.

During model development, the sparsity of matrix A used for parameter calculation is also investigated. Fig. 7 illustrates the sparsity patterns of the 2 × 2 model, 15 × 15 model, 30 × 2 and 50 × 2 model configurations, respectively, where each point in the chart denotes the location of a non-zero array element. When the system of linear equations is arranged in a certain order, the elements of matrix A occupy some diagonals, see Fig. 7 (a), (b). That makes the system easy to solve. Even when considering the battery with a long-band layout, the diagonal arrangement of matrix sparsity remains, as shown in Figs. 7 (c) and 7 (d). Certainly, the number of matrix elements has changed when transitioning from 30:2 to 50:2, but the overall arrangement remains concise and clear. The matrix elements, corresponding to a closed-loop set of Kirchhoff equations, have positive and negative values. The red dots in the plot represent positive values, and the blue dots represent negative values. Fig. 7 illustrates the high sparsity of the matrix in this model.

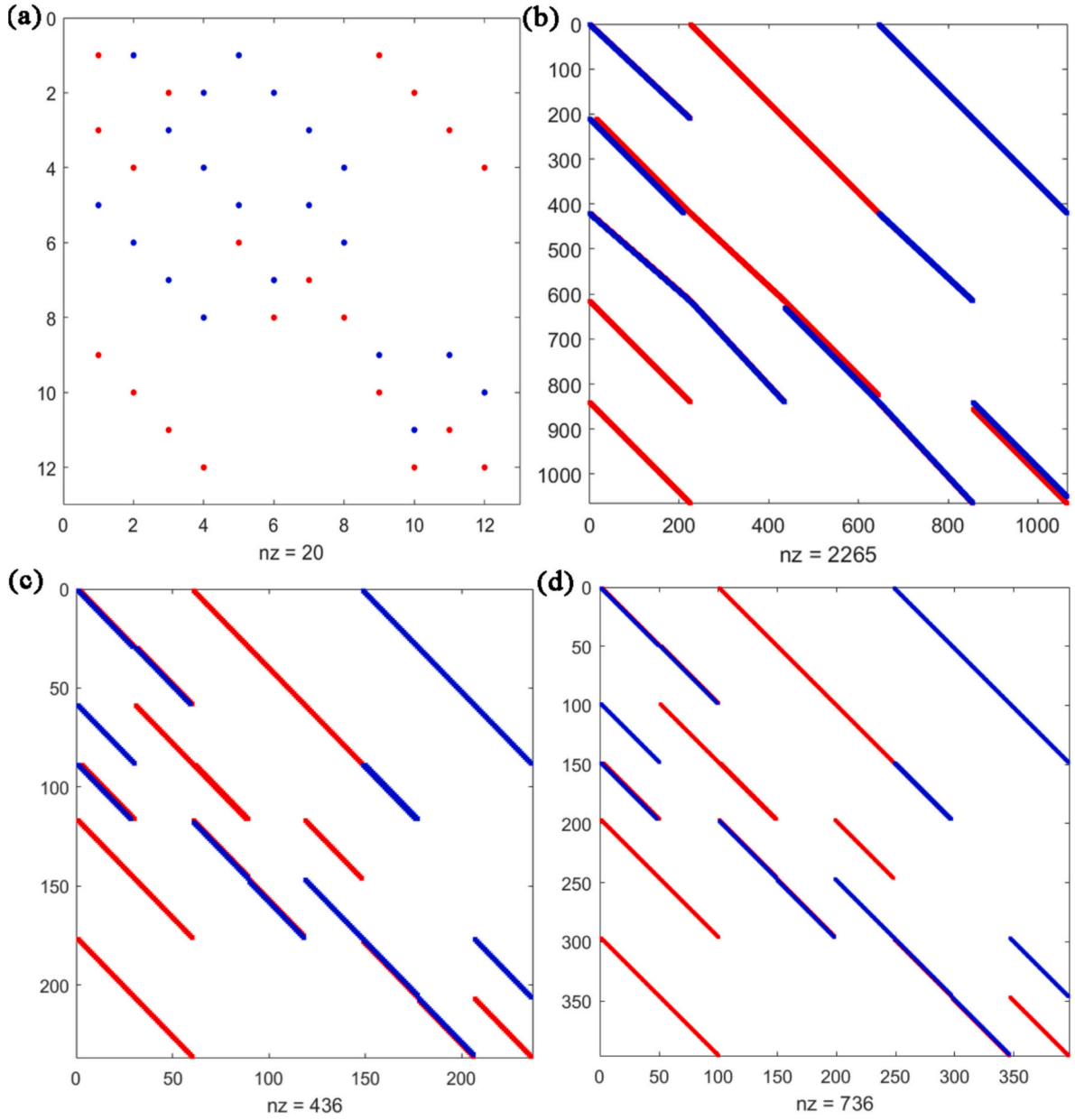


**Fig. 7.** Sparsity of matrix A of (a) 2 × 2 model, (b) 15 × 15 model, (c) 30 × 2 model and (d) 50 × 2 model, respectively.

Therefore, the proposed model can reduce storage requirements and mitigate the cumulative impact of calculation errors, thereby enhancing overall solving efficiency [26]. Additionally, the sparse matrix formulation directly maps to the topological architecture of the circuits, thereby enhancing model fidelity by preserving connections with common physics [27].

## 5. Conclusion

The influence of current collector resistance on the SoC and current density distribution within lithium-ion batteries was systematically investigated using Kirchhoff's circuit laws with a simple discretization. That approach offers notable advantages in terms of computational simplicity and resource efficiency. Simulation results indicate that an increasing resistance disparity between cathodic and anodic current collectors exacerbates the inhomogeneity of SoC distribution. Furthermore, the geometric dimensions of current collectors significantly modulate this distributional behavior. Inhomogeneous current density and SoC profiles induce uneven utilization of electrode materials, thereby accelerating localized aging mechanisms in lithium-ion batteries. The proposed model can be synergistically integrated with existing models that neglect current collector effects to achieve enhanced simulation accuracy. Its methodological framework exhibits generality across diverse battery chemistries and configurations, offering a novel analytical lens for evaluating the impact of design parameters and operational conditions on critical electrochemical distributions, which contributes to the rational design of next-generation batteries characterized by improved energy density, safety, and longevity.

## CRediT authorship contribution statement

**Zhenya Wang:** Writing – original draft, Visualization, Validation, Software, Investigation, Formal analysis, Data curation. **Dmitri L. Danilov:** Writing – review & editing, Supervision, Methodology, Conceptualization. **Jingjing Zhou:** Resources, Project administration. **Meng Zheng:** Supervision, Software, Funding acquisition. **Yi Huang:**

Formal analysis. **Tao Chen:** Resources. **Rüdiger-A. Eichel:** Supervision, Project administration. **Peter H.L. Notten:** Supervision, Project administration.

## Declaration of competing interest

The authors declare that they have no known competing financial interests or personal relationships that could have appeared to influence the work reported in this paper.

## Acknowledgments

Dr. D.L. appreciates the support from the grant ProMoBiS (grant Number 03ETE046C, BMBF, Germany).

## Data availability

Data will be made available on request.

## References

[1] V. Foster, P.A. Trotter, S. Werner, M. Niedermayer, Y. Mulugetta, P. Achakulwisut, A. Brophy, N.K. Dubash, S. Fankhauser, A. Hawkes, S. Hirmer, S. Jenkins, S. Loni, A. McGivern, K. Nanthavong, B. Probst, S. Pye, V. Russo, G. Semieniuk, C. Shenga, V. Sridharan, S. Srivastav, Y. Sokona, L.S. Croxatto, P. Yang, Development transitions for fossil fuel-producing low and lower–middle income countries in a carbon-constrained world, Nat. Energy (2024) 1–9, https://doi.org/10.1038/s41560-023-01440-3.

[2] F. Wang, J.D. Harindintwali, Z. Yuan, M. Wang, F. Wang, S. Li, Z. Yin, L. Huang, Y. Fu, L. Li, S.X. Chang, L. Zhang, J. Rinklebe, Z. Yuan, Q. Zhu, L. Xiang, D.C. W. Tsang, L. Xu, X. Jiang, J. Liu, N. Wei, M. Kästner, Y. Zou, Y.S. Ok, J. Shen, D. Peng, W. Zhang, D. Barceló, Y. Zhou, Z. Bai, B. Li, B. Zhang, K. Wei, H. Cao, Z. Tan, L. Zhao, X. He, J. Zheng, N. Bolan, X. Liu, C. Huang, S. Dietmann, M. Luo, N. Sun, J. Gong, Y. Gong, F. Brahushi, T. Zhang, C. Xiao, X. Li, W. Chen, N. Jiao, J. Lehmann, Y.-G. Zhu, H. Jin, A. Schäffer, J.M. Tiedje, J.M. Chen, Technologies and perspectives for achieving carbon neutrality, The Innovation 2 (2021), https://doi.org/10.1016/j.xinn.2021.100180.

[3] L. Köbbing, A. Latz, B. Horstmann, Growth of the solid-electrolyte interphase: Electron diffusion versus solvent diffusion, J. Power Sources 561 (2023) 232651, https://doi.org/10.1016/j.jpowsour.2023.232651.

[4] H. Zhang, C. Li, G.G. Eshetu, S. Laruelle, S. Grugeon, K. Zaghib, C. Julien, A. Mauger, D. Guyomard, T. Rojo, N. Gisbert-Trejo, S. Passerini, X. Huang, Z. Zhou, P. Johansson, M. Forsyth, From solid-solution electrodes and the rocking-chair concept to today's batteries, Angew. Chem. Int. Ed. 59 (2020) 534–538, https://doi.org/10.1002/anie.201913923.

[5] X. Li, J.T. Kim, J. Luo, C. Zhao, Y. Xu, T. Mei, R. Li, J. Liang, X. Sun, Structural regulation of halide superionic conductors for all-solid-state lithium batteries, Nat. Commun. 15 (2024) 53, https://doi.org/10.1038/s41467-023-43886-9.

[6] L. Jia, J. Zhu, X. Zhang, B. Guo, Y. Du, X. Zhuang, Li–solid electrolyte interfaces/interphases in all-solid-state Li batteries, Electrochem. Energy Rev. 7 (2024) 12, https://doi.org/10.1007/s41918-024-00212-1.

[7] N. Zhang, Q. He, L. Zhang, J. Zhang, L. Huang, X. Yao, Homogeneous Fluorine Doping toward Highly Conductive and Stable Li10GeP2S12 Solid Electrolyte for all-Solid-State Lithium Batteries, (n.d.). doi: https://doi.org/10.1002/adma.202408903.

[8] L. Cui, S. Zhang, J. Ju, T. Liu, Y. Zheng, J. Xu, Y. Wang, J. Li, J. Zhao, J. Ma, J. Wang, G. Xu, T.-S. Chan, Y.-C. Huang, S.-C. Haw, J.-M. Chen, Z. Hu, G. Cui, A cathode homogenization strategy for enabling long-cycle-life all-solid-state lithium batteries, Nat. Energy 9 (2024) 1084–1094, https://doi.org/10.1038/s41560-024-01596-6.

[9] V. Laue, F. Röder, U. Krewer, Joint structural and electrochemical modeling: impact of porosity on lithium-ion battery performance, Electrochim. Acta 314 (2019) 20–31, https://doi.org/10.1016/j.electacta.2019.05.005.

[10] M. Zhuo, G. Offer, M. Marinescu, Degradation model of high-nickel positive electrodes: effects of loss of active material and cyclable lithium on capacity fade, J. Power Sources 556 (2023) 232461, https://doi.org/10.1016/j.jpowsour.2022.232461.

[11] N. Kazemi, D.L. Danilov, L. Haverkate, N.J. Dudney, S. Unnikrishnan, P.H. L. Notten, Modeling of all-solid-state thin-film Li-ion batteries: accuracy improvement, Solid State Ionics 334 (2019) 111–116, https://doi.org/10.1016/j.ssi.2019.02.003.

[12] J. Sturm, A. Rheinfeld, I. Zilberman, F.B. Spingler, S. Kosch, F. Frie, A. Jossen, Modeling and simulation of inhomogeneities in a 18650 nickel-rich, silicon-graphite lithium-ion cell during fast charging, J. Power Sources 412 (2019) 204–223, https://doi.org/10.1016/j.jpowsour.2018.11.043.

[13] L.H.J. Raijmakers, D.L. Danilov, R.-A. Eichel, P.H.L. Notten, An advanced all-solid-state Li-ion battery model, Electrochim. Acta 330 (2020) 135147, https://doi.org/10.1016/j.electacta.2019.135147.

[14] D. Danilov, R.A.H. Niessen, P.H.L. Notten, Modeling All-Solid-State Li-Ion Batteries, J. Electrochem. Soc. 158 (2010) A215, https://doi.org/10.1149/1.3521414.

[15] A. Bates, S. Mukherjee, N. Schuppert, B. Son, J.G. Kim, S. Park, Modeling and simulation of 2D lithium-ion solid state battery: effects of materials and geometry on the performance of SSB, Int. J. Energy Res. 39 (2015) 1505–1518, https://doi.org/10.1002/er.3344.

[16] S.D. Fabre, D. Guy-Bouyssou, P. Bouillon, F. Le Cras, C. Delacourt, Charge/discharge simulation of an all-solid-state thin-film battery using a one-dimensional model, J. Electrochem. Soc. 159 (2011) A104–A115, https://doi.org/10.1149/2.041202jes.

[17] Y. Xie, W. Li, Y. Yang, F. Feng, A novel resistance-based thermal model for lithium-ion batteries, Int. J. Energy Res. 42 (2018) 4481–4498, https://doi.org/10.1002/er.4193.

[18] S.R. Anton, A. Erturk, D.J. Inman, Multifunctional self-charging structures using piezoceramics and thin-film batteries, Smart Mater. Struct. 19 (2010) 115021, https://doi.org/10.1088/0964-1726/19/11/115021.

[19] N. Kuwata, J. Kawamura, K. Toribami, T. Hattori, N. Sata, Thin-film lithium-ion battery with amorphous solid electrolyte fabricated by pulsed laser deposition, Electrochem. Commun. 6 (2004) 417–421, https://doi.org/10.1016/j.elecom.2004.02.010.

[20] Z. Wang, D.L. Danilov, R.-A. Eichel, P.H.L. Notten, Modeling the resistance of thin-film current collectors in thin-film batteries, J. Electrochem. Soc. 170 (2023) 020514, https://doi.org/10.1149/1945-7111/acb855.

[21] P. Taheri, A. Mansouri, B. Schweitzer, M. Yazdanpour, M. Bahrami, Electrical constriction resistance in current collectors of large-scale Lithium-ion batteries, J. Electrochem. Soc. 160 (2013) A1731–A1740, https://doi.org/10.1149/2.041310jes.

[22] S.V. Erhard, P.J. Osswald, P. Keil, E. Höffer, M. Haug, A. Noel, J. Wilhelm, B. Rieger, K. Schmidt, S. Kosch, F.M. Kindermann, F. Spingler, H. Kloust, T. Thoennessen, A. Rheinfeld, A. Jossen, Simulation and measurement of the current density distribution in Lithium-ion batteries by a multi-tab cell approach, J. Electrochem. Soc. 164 (2017) A6324–A6333, https://doi.org/10.1149/2.0551701jes.

[23] U.S. Kim, C.B. Shin, C.-S. Kim, Modeling for the scale-up of a lithium-ion polymer battery, J. Power Sources 189 (2009) 841–846, https://doi.org/10.1016/j.jpowsour.2008.10.019.

[24] G. Zhang, C.E. Shaffer, C.-Y. Wang, C.D. Rahn, In-situ measurement of current distribution in a Li-ion cell, J. Electrochem. Soc. 160 (2013) A610, https://doi.org/10.1149/2.046304jes.

[25] F. Brauchle, F. Grimsmann, O. von Kessel, K.P. Birke, Direct measurement of current distribution in lithium-ion cells by magnetic field imaging, J. Power Sources 507 (2021) 230292, https://doi.org/10.1016/j.jpowsour.2021.230292.

[26] J. Gao, W. Ji, F. Chang, S. Han, B. Wei, Z. Liu, Y. Wang, A Systematic Survey of General Sparse Matrix-matrix Multiplication, ACM Comput. Surv. 55 (2023), https://doi.org/10.1145/3571157, 244:1–244:36.

[27] J. Li, S. Ren, Y. Li, L. Yang, Y. Yu, R. Ni, H. Zhou, H. Bao, Y. He, J. Chen, H. Jia, X. Miao, Sparse matrix multiplication in a record-low power self-rectifying memristor array for scientific computing, Sci. Adv. 9 (2023) eadf7474, https://doi.org/10.1126/sciadv.adf7474.